Paper: ASAT-15-014-MS

15th International Conference on
AEROSPACE SCIENCES & AVIATION TECHNOLOGY,
ASAT - 15 – May 28 - 30, 2013, Email: asat@mtc.edu.eg ,
Military Technical College, Kobry Elkobbah, Cairo, Egypt,
Tel: +(202) 24025292 –24036138, Fax: +(202) 22621908

The Effect of Stacking Sequence and Coupling Mechanisms on Eigen-Nature of Composite Shafts

S. M. Ghoneam*, A. A. Hamada†, M. I. EL-Elamy‡

Abstract: Composite materials have interesting properties such as high strength-to-weight ratio and relatively high damping characteristics compared to metals which make them very attractive for rotating systems. They also provide designers with the possibility of obtaining predetermined behaviors in terms of position of critical speed by changing the arrangement of the different composite layers orientation and number of plies.
The composite rotating shafts used will be fabricated using hand layout technique by filament winding technique. Glass fiber (E-Glass) as reinforced with a matrix of polyester resin and hardener will be used to construct the composite layers needed. Five cases will be studied using composite shafts wounded by different layers of composite materials namely; different stacking sequence, fiber orientation angles, (***L/D***) ratio, boundary condition and finally various types of fiber volume fraction. In the theoretical part, the validity of the proposed theoretical model for evaluating the dynamic response of composite shafts will be examined utilizing the equivalent modulus beam theory (EMBT).
In the experimental part, the frequency of composite shaft specimens will be measured by self-excitation and so critical speed of the rotating shaft will be determined by using the (TM1 MKII Whirling) machine apparatus.
The numerical finite element technique is utilized to compute the eigen pairs of laminated composite shafts. A finite element model FEM has been developed to formulate the stiffness matrices using lamination theory. These matrices take into account the effects of axial, flexural and shear deformation on the eigen-nature of rotating composite shaft.
Eigen natures of composite shafts were estimated through modal testing and are compared with (EMBT) results.
The comparison between the numerical and experimental results proves that the suggested finite element models of the composite shaft provide an efficient accurate tool for the dynamic analysis of rotating composite shaft.

Keywords: Stacking sequence, modeling, finite element, EMBT, eigen-nature.

1. Introduction

Composite materials are widely used as alternatives for conventional materials because of their desirable and tailorable properties that could not be achieved by either of the constituent material acting alone. Their superior strength-to-weight ratio, greater specific stiffness, and properties such as good wear resistance, long fatigue life, durability, thermal, electrical, and acoustical insulation, etc., have made them attractive alternatives for conventional materials in

* Department of Production Engineering and Mechanical Design, Faculty of Engineering, Menoufiya University, Shebin El-Kom, Egypt; Ghoneam22000@Yahoo.com
† a_hamed_59@yahoo.com
‡ mamdouhelimi@yahoo.com

a wide variety of products. The most common example of a composite material is reinforcing fibers embedded in a matrix. Fiber orientation in each layer as well as the stacking sequence of various layers can be controlled to generate a wide range of physical and mechanical properties for the composite laminate. The fibers form the principal load carrying members, while the surrounding matrix acts as a load transfer medium between the fibers. The surrounding matrix also keeps the fibers in desired location and orientation and also protects them from environmental damages due to temperature and humidity.

Rotating flexible shafts are important machine elements, commonly used in many mechanical systems. These include reciprocating and centrifugal compressors, and lathe, grinding and milling machines which employ rotating elements as cutting tools. The rotating shaft may also be used as a means of power transmission in industrial machines such as gas turbines, turbo generators, aircraft engines, automobiles, medical equipment, household accessories and internal combustion engines [1]. In each case, the vibration control and stability of the rotating shaft are essential for the success of the machine operation, the precision of the cutting tools or the high efficiency of energy transmission in engines. The stability of rotating shafts under both conservative and non-conservative forces has been treated by Bolotin [2].

Rotating shafts are used for power transmission in many modern machines. Accurate prediction of dynamics of rotating shafts is necessary for a successful design. Free vibrations analysis is one of the important steps in rotor-dynamics. Grybos [3] considered the effect of shear deformation and rotary inertia of a rotor on its critical speeds. Choi et al. [4] presented the consistent derivation of a set of governing differential equations describing the flexural and the torsional vibrations of a rotating shaft where a constant compressive axial load was acted on it. Jei and Leh [5] investigated the whirl speeds and mode shapes of a uniform asymmetrical Rayleigh shaft with asymmetrical rigid disks and isotropic bearings. Free damped flexural vibrations analysis of composite cylindrical tubes was carried out by Singh and Gupta [6], where they used beam and shell theories. Sturla and Argento [7] studied the free and forced response of a viscoelastic spinning Rayleigh shaft. Melanson and Zu [8] studied the free vibrations and stability of internally damped rotating shafts with general boundary conditions. Kim et al. [9] studied the free vibrations of a rotating tapered composite Timoshenko shaft. Hosseini et al. [10] studied the free vibrations of an in-extensional simply supported rotating shaft with nonlinear curvature and inertia are considered. Rotary inertia and gyroscopic effects are included, but shear deformation is neglected.

Accurate prediction of damping characteristics of rotor systems is therefore fundamental in the design of rotating machines as it provides estimations on safe-ranges of speeds of rotation. Over the last few years, many studies have focused on predicting critical speeds, natural frequencies, unbalance responses and, in particular, instability thresholds. Newkirk [11] observed that rotor-disk systems would undergo violent whirling at the first natural frequency at speeds above the first critical speed. Kimball [12] showed that internal damping destabilizes the whirling motion if the rotation speed of the rotor exceeds the first critical speed. In addition, Bucciarelli [13] showed that the instability criterion based on the ratio of energy dissipated between internal and external damping is inaccurate and that internal forces can produce instability by coupling spin and whirl motions.

Classical results have been obtained and showed that rotor stability is improved by increasing external damping, whereas, increasing internal damping may reduce the instability threshold. However, most of the published studies deal with metal rotating structures and remain exclusively numerical without precise estimations of internal damping. Several finite element formulations have been performed for the analysis of composite shafts. These formulations

are based on homogenized beam and shell theories. The equivalent modulus beam theory (EMBT), which is widely used for the dynamic analysis of composite shafts, was firstly introduced by Tsai [14].

Rastogi [15] used a hybrid of carbon/epoxy and glass/epoxy to optimize the cost versus performance requirements. He analyzed and designed a composite drive shaft using two approaches. The first approach is closed-form analytical expressions for the critical speed, torsional strength and buckling strength, which was utilized to develop a preliminary design tool. The effect of fiber orientation angle on the fatigue strength of composite tubes was discussed by many researchers [16–18] but, on the other hand, the effect of stacking sequence on the torsional fatigue strength is not available. Bert and Kim [19] carried out an analytical solution to compute torsional buckling of composite drive shafts. They calculated the torsional buckling load of composite drive shafts with various lay-ups with good accuracy by considering the effect of off-axis stiffness and flexural moment. Their theory can predict the torsional buckling of composite drive shafts under pure torsion and combined torsion and bending. Chen and Peng [20] performed numerical simulation using a finite element method to study the stability of composite shafts under combined loading conditions. They predicted the critical axial load of a thin walled composite drive shaft under rotation. Badie et al. [21] studied the effect of fiber orientation angles and stacking sequence on the torsional stiffness, natural frequency, buckling strength, fatigue life and failure modes of composite tubes. Finite element analysis (FEA) has been used to predict the fatigue life of composite drive shaft (CDS) using linear dynamic analysis for different stacking sequences.

From previous review we can note that many papers introduced FEM to describe composite model studying a single fixation such as simply supported, while a group of papers was interested to study a limit number of lamina orientation. Other authors applied equivalent modulus beam theory (EMBT). The theory is generalized to include bending–twisting, shear–normal and bending–stretching coupling effects. To account for the locations of different plies and their stacking sequence, longitudinal and inplane shear moduli are taken in the ply level.
A Bresse–Timoshenko beam with transverse shear deformation, rotary inertia and gyroscopic effects included is considered from many authors to describe and formulate the stiffness and inertia effects of composite shaft system.

The main objectives of the present paper are studying the effect of staking sequences and coupling mechanisms on the dynamic analysis (frequency, damping factor and mode shape) of composite shaft.

In the theoretical part, the validity of the proposed theoretical model for evaluating the dynamic response of composite shafts will be examined utilizing the finite element technique.

In the experimental part, the frequency of composite shaft specimens will be measured by self-excitation and so critical speed of the rotating shaft will be determined by using the (TM1 MKII Whirling) machine apparatus.

The effects of stacking sequences and anisotropic parameters on eigen-nature have been analyzed. This can be useful for designing the composite shafts for different requirements. Half-power bandwidth method used for measure damping nature has been demonstrated for estimating the damping nature at any speed which can be quite a valuable tool for estimating the damping at different speeds, it can be concluded that inclusion of layer along the transverse direction into fiber/polyester material is a good option for manufacturing stiffer shafts.

The comparison between the numerical and experimental results proves that the suggested finite element models of the composite shaft provide an efficient accurate tool for the dynamic analysis of rotating composite shaft.

2. Materials and Production of Laminates Composite Shaft

Glass fiber is used as reinforcement in the form of bidirectional fabric (Standard E-Glass Fiberglass) and polyester with catalyst addition as matrix for the composite material. The mechanical properties of the composite are calculated analytically using the mixture rule [22]. Through hand lay-up process followed by a cure process, five sets of symmetrical laminates with a total of five layers each one are produced:

Set1: ***[0/0/0/0/0]***, Set2: ***[0/45/0/45/0]***, Set3: ***[0/90/0/09/0]*** Set4: ***[45/45/0/45/45]*** and Set5: ***[90/90/0/90/90]***. The numbers mentioned in the above sets indicates the angle of fiber inclination measured by degrees.

After the cure process, the laminated composite shaft dimensions with length of L = ***790 mm*** and ***D= 18.3 mm*** diameter and various ***L/D*** ratios are ***20***, ***30*** and ***40***.

A typical specimen made from fiber reinforced plastic FRP composite shafts formed from five plies with 1mm thickness for each ply is shown in Fig. 1. Three composite levels were selected for each code number. These are specimens with low fiber volume fraction V_f **= 25%** and two levels of average fiber volume fraction V_f **= 45 %** and **65%**. The fiber volume fraction in the specimens is determined experimentally, using the firing processes method [23]

In order to study the effect of lamina orientation and staking sequence on the modal parameters, five code numbers of the specimens were fabricated and stated for each fiber volume fraction.

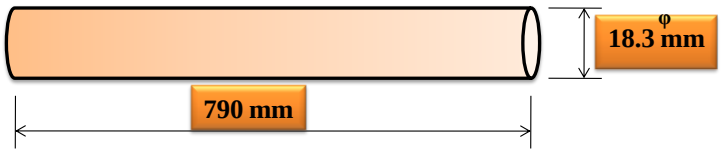

Fig. 1 Three-dimensional specimen of composite shaft.

3. Theoretical Investigation

The present theoretical study is used to compute the mechanical properties of laminated composite shaft using mixture rule shown in Fig. 2. The laminate extensional, coupling and bending stiffness matrices of composite symmetric laminated composite shaft with different predetermined lamina orientations are computed on the basis of the classical lamination theory [24]. The material properties of each ply are summarized in Table 1

3.1 Finite Element Formulation

The rotor model is based on the finite element approach. The distributed properties of shafting sections are modeled by the theory of Timoshinko beam (circular) element that accounts for rotary inertia, gyroscopic moments, internal damping and shear deformation. The cylindrical composite shaft shown in Fig. 3 is assumed to be built up by a number of lamina perfectly bonded together. There are no relative displacements between adjacent layers.

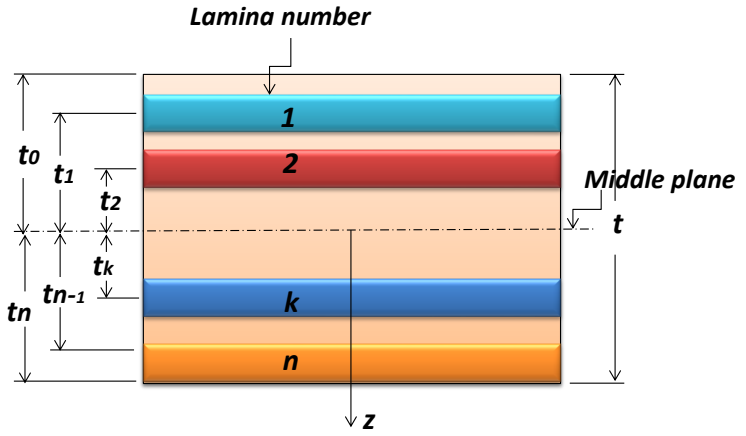

Fig. 2 Composite laminated shaft [25].

Table 1 Mechanical properties of the composite shaft

Elastic modulus	E_{11}, [GPa]	E_{22}, [GPa]	G_{12}, [GPa]	v_{12}	v_{21}
$V_f = 25\%$	20.75	4.60	2.29	0.27	0.06
$V_f = 45\%$	34.51	6.12	2.58	0.29	0.052
$V_f = 65\%$	48.3	9.2	2.9	0.302	0.058

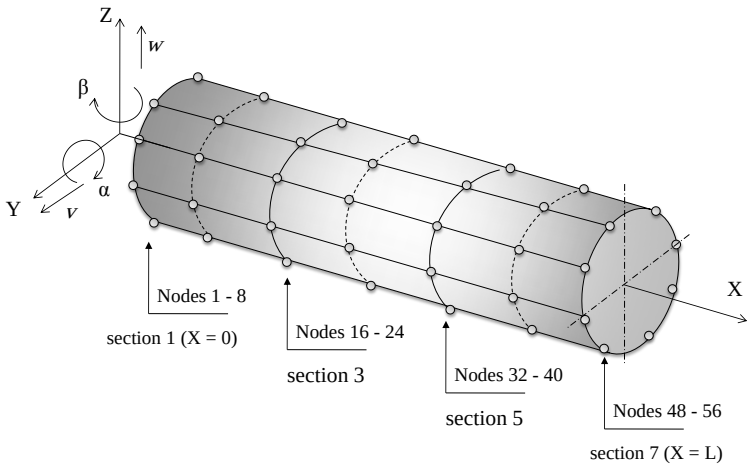

Fig. 3 Finite element of composite shaft.

The finite element used has eight nodes as shown in Fig. 3. For each node, the element has four degrees of freedom: two displacements v and w, and two slopes about the y and z axes denoted, respectively α and β. In this case, the shaft axis is x. Referring to Fig. 3, the displacement field at a point in the element can be expressed in global coordinates as

$$\begin{aligned} [M]_e &= [m]_d + [m]_c \\ [C]_e &= [c]_g + [c]_d \\ [K]_e &= [k]_d + [k]_c \end{aligned} \tag{1}$$

where $[m]_d$ is the translational mass matrix, $[m]_c$ is the rotational mass matrix,$[c]_g$ is the gyroscopic matrix, $[c]_d$ is a damping of composite including bearing $[k]_d$ is the stiffness matrix and $[k]_c$ is the stiffness matrix including the effects of concentrated bearing properties. The reader is referred to [26] for details of these matrices.

The Eigen-frequency can be then evaluated from the solution of the characteristic equation for composite shaft given by:

$$[-\Omega^2[M]_e + i\Omega[C]_e + [K]_e]\{X\} = \{0\} \tag{2}$$

In view of Eqn. (2), the program has been coded into computer using Matlab (***7.1***). The program computes the mass matrices and stiffness matrices of any orientation and fixation of the composite shaft. It computes the Eigen-values and Eigen-vectors. The Eigen-values are obtained by computing the roots of the characteristic polynomial of any real square matrix in an iterative manner with an accuracy of $\boldsymbol{10^{-6}}$ for four fixations namely; ***C-C***, ***C-S***, ***S-S*** and ***C-F,*** where: C = clamped, S = simply-support and F = free.

3.2. Modified Equivalent Modulus Beam Theory

A Bresse–Timoshenko beam with transverse shear deformation, rotary inertia and gyroscopic effects included is considered. The theory is generalized to include bending–twisting, shear–normal and bending–stretching coupling effects. To account for the locations of different plies and their stacking sequence, longitudinal and in-plane shear moduli are taken in the ply level.

3.2.1. Formulation

Consider shaft as shown in Fig. 3. The displacement field is described by the transverse displacements, ***w*** and ***v*** measured in the ***z*** and ***y*** directions, the bending slopes ***α*** and ***β*** in the ***x–z*** and ***x–y*** planes and ***ϕ*** is the shaft twist angle. The quantities ***w, v, α, β*** and ***ϕ*** are assumed to be time dependent and are expressed as

$$w = \bar{w}e^{i\Omega t}\ , = \bar{v}e^{i\Omega t}\ ,\alpha = \bar{\alpha}e^{i\Omega t}, = \bar{\beta}e^{i\Omega t}\ , \phi = \bar{\phi}e^{i\Omega t} \tag{3}$$

where ***Ω*** is the whirl frequency

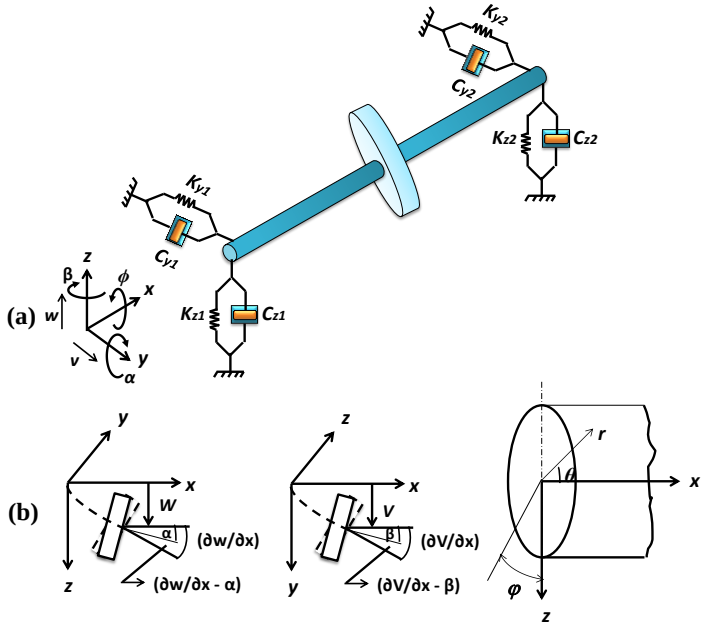

Fig. 3 (a) Rotor-bearing system model, (b) Cartesian coordinates

The strain energy of the shaft including bending in two planes, shear deformation, torsional energy can be expressed and strain energy for right and lift bearing [26] as

$$U = \frac{1}{2}\int_0^l \left\{ k_B \left[\left(\frac{\partial \alpha}{\partial x}\right)^2 + \left(\frac{\partial \beta}{\partial x}\right)^2 \right] + k_S \left[\left(\frac{\partial w}{\partial x} - \alpha\right)^2 + \left(\frac{\partial v}{\partial x} - \beta\right)^2 \right] + k_T \left(\frac{\partial \phi}{\partial x}\right)^2 \right\} dx + \frac{1}{2}\sum_{i=1}^{n} K_{zi} w^2 + \frac{1}{2}\sum_{i=1}^{n} K_{yi} v^2 \quad (4)$$

where k_B is the bending stiffness coefficient which can be given [27] by

$$k_B = \frac{\pi}{4}\sum_{k=1}^{n} \bar{Q}_{11}^{(k)} \left[R_{(k)}^4\right] \quad (5)$$

The torsional stiffness coefficient $\boldsymbol{k_T}$ [27] is

$$k_T = \frac{\pi}{4}\sum_{k=1}^{n} \bar{Q}_{66}^{(k)} \left[R_{(k)}^4\right] \quad (6)$$

and the shear stiffness coefficient $\boldsymbol{k_S}$ is given by

$$k_S = \grave{k}\, A\, G_{X\theta} \quad (7)$$

where $\boldsymbol{\grave{k}}$ is the shear correction factor, ***Kyi*** and ***Kzi*** are the stiffness coefficient for bearing in y and z direction respectively.

In Eqs. (5) and (6), $\boldsymbol{R_{(k)}^4}$, $\boldsymbol{\bar{Q}_{11}^{(k)}}$ and $\boldsymbol{\bar{Q}_{66}^{(k)}}$ are the outer radii, longitudinal and shear stiffness coefficients of the k[th] ply, respectively.

The total kinetic energy is the sum of the kinetic energies the shaft and the discs mounted on it. This can be expressed [26] as

$$T = \frac{1}{2}\int_0^l \left[\rho A(\dot{w}^2 + \dot{v}^2) + \rho I\left(\dot{\alpha}^2 + \dot{\beta}^2\right) + \rho I_P \dot{\phi}^2 + 2\rho I_P \omega \dot{\alpha}\beta\right] dx + \frac{1}{2}\sum_{i=1}^{ND}\left[M_{Di}(\dot{w}(x_i)^2 + v(x_i)^2) + I_{DTi}\left(\dot{\alpha}(x_i)^2 + \dot{\beta}(x_i)^2\right) + 2I_{DPi}\omega\dot{\alpha}(x_i)\beta(x_i)\right] \quad (8)$$

Here $\boldsymbol{\rho}$ is the mass density of the shaft material, $\boldsymbol{A}$, $\boldsymbol{I}$ and $\boldsymbol{Ip}$ are area, lateral and polar area moments of inertia of the shaft cross-section. $\boldsymbol{M_{Di}}$, $\boldsymbol{I_{DTi}}$ and $\boldsymbol{I_{DPi}}$ are mass, lateral and polar mass moments of inertia of the $\boldsymbol{i^{th}}$ disc, respectively. The rotational angular speed of the shaft is $\boldsymbol{\omega}$. The first, second, third and fourth set of terms within the integral sign give the effect of translatory, rotary and torsional inertia, and gyroscopic moment of the shaft. The four terms within the summation sign give the same effects for the discs mounted on the shaft.

Table 2 Bearing stiffness data

Bearing stiffness	K_{z1} (N/m)	K_{y1} (N/m)	K_{z2} (N/m)	K_{y2} (N/m)
Value	1×10^7	1×10^7	1×10^7	1×10^7

3.2.2. Solution equations

The series solution functions are assumed for ***w, v, α, β*** and ***ϕ*** in the form

$$\bar{w}(x) = \sum_{j=1}^{n} W_j \sin\frac{j\pi x}{l}, \quad \bar{v}(x) = \sum_{j=1}^{n} V_j \sin\frac{j\pi x}{l}, \quad \bar{\beta}(x) = \sum_{j=1}^{n} B_j \cos\frac{j\pi x}{l}$$
$$\bar{\alpha}(x) = \sum_{j=1}^{n} A_j \cos\frac{j\pi x}{l}, \quad \bar{\phi}(x) = \sum_{j=1}^{n} \Phi_j \cos\frac{j\pi x}{l} \quad (9)$$

Here ***n*** is the total number of terms in the series solutions. The above functions satisfy geometric boundary conditions at ***x = 0*** and ***x = l***: The Lagrangian ***L = U - T*** is set up from strain and kinetic energies and made stationary with respect to the solution coefficients, i.e.

$$\frac{\partial L}{\partial W_j} = 0,\ \frac{\partial L}{\partial V_j} = 0,\ \frac{\partial L}{\partial A_j} = 0,\ \frac{\partial L}{\partial B_j} = 0,\ \frac{\partial L}{\partial \Phi_j} = 0 \tag{10}$$

The time dependence cancels out in all the terms and a set of ***5n*** simultaneous algebraic equations in the form of a quadratic eigenvalue problem is obtained as

$$\left[-\Omega^2[M] + i\Omega[C] + [K]\right]\{X\} = \{0\} \tag{11}$$

Here the matrix [C] involves the contribution due to the gyroscopic effect and is dependent on rotational speed. The eigenvector {X} is given by

$$\{X\} = [W_1, W_2, \dots, W_n \quad V_1, V_2, \dots, V_n \quad A_1, A_2, \dots, A_n \quad B_1, B_2, \dots, B_n \quad \Phi_1, \Phi_2, \dots, \Phi_n]^T \tag{12}$$

3.3. Improvement to Include Different Coupling Mechanisms

Several refinements have been made to account for different coupling mechanisms effects, namely, Poisson's effect, shear–normal and bending–twisting coupling effects. Generally, the strain energy in the shaft is given by

$$U = \sum_{k=1}^{n} U^k = \frac{1}{2}\sum_{k=1}^{n} \int [\sigma^k]\{\varepsilon^k\}\, dv \tag{13}$$

The summation is taken over all the plies contained in the laminate, and

$$[\sigma]^k = \begin{Bmatrix}\sigma_{xx}\\ \sigma_{\theta\theta}\\ \tau_{x\theta}\end{Bmatrix}^k = \begin{bmatrix}\bar{Q}_{11} & \bar{Q}_{12} & \bar{Q}_{16}\\ \bar{Q}_{12} & \bar{Q}_{22} & \bar{Q}_{26}\\ \bar{Q}_{16} & \bar{Q}_{26} & \bar{Q}_{66}\end{bmatrix}^k \begin{Bmatrix}\varepsilon_{xx}\\ \varepsilon_{\theta\theta}\\ \varepsilon_{x\theta}\end{Bmatrix}^k \tag{14}$$

Here σ_{xx} and $\sigma_{\theta\theta}$ are inplane normal and hoop stresses and $\tau_{x\theta}$ is the inplane shear stress, ε_{xx} and $\varepsilon_{\theta\theta}$ are the inplane normal and hoop strains and $\varepsilon_{x\theta}$ is the inplane shear strain in x and y coordinates as shown in Fig. 3b. $[\bar{Q}]$ is the transformed stiffness matrix of the k^{th} ply.

3.3.1. Improvement to Include Poisson's Coupling Effect

In a thin single ply, shear effect is negligible and bending–stretching and shear–normal coupling effects are not present. However, in calculating strain energy, ε_θ is taken to be zero, which implies some effective stress occurs in θ-direction. But in the actual case no such stress acts. Thus, imposition of the condition of no cross-section deformation results in no strain condition in the circumferential direction and this gives higher frequency values. The circumferential stress in each ply is assumed to be zero, thus from Eq. (14),

$$\sigma_{\theta\theta}^{(k)} = \bar{Q}_{22}^{(k)}\varepsilon_{\theta\theta}^{(k)} + \bar{Q}_{12}^{(k)}\varepsilon_{xx}^{(k)} = 0$$

This gives

$$\varepsilon_{\theta\theta}^{(k)} = -\frac{\bar{Q}_{12}^{(k)}\varepsilon_{xx}^{(k)}}{\bar{Q}_{22}^{(k)}}$$

Also from Eq. (12) we have

$$\sigma_{xx}^{(k)} = \bar{Q}_{11}^{(k)}\varepsilon_{\theta\theta}^{(k)} + \bar{Q}_{12}^{(k)}\varepsilon_{xx}^{(k)}$$

Substituting for $\varepsilon_{\theta\theta}^{(k)}$ from above

$$\sigma_{xx}^{(k)} = \left(\frac{\bar{Q}_{11}^{(k)} - \left(\bar{Q}_{12}^{(k)}\right)^2}{\bar{Q}_{22}^{(k)}}\right)\varepsilon_{xx}^{(k)} = \bar{Q}_{11\,m}^{(k)}\varepsilon_{xx}^{(k)} \tag{15}$$

where

$$\bar{Q}_{11\,m}^{(k)} = \left(\frac{\bar{Q}_{11}^{(k)} - \left(\bar{Q}_{12}^{(k)}\right)^2}{\bar{Q}_{22}^{(k)}}\right) \tag{16}$$

Thus the value of $\bar{Q}_{11}$ is updated to account for Poisson's effect according to Eq. (16).

3.3.2. Improvement to Include Shear–Normal Coupling Effect

In conventional filament winding procedure the fibers at winding angles ±***θ*** are interwoven in the same ply; similarly for configurations in which corresponding to ***+θ*** orientation ply above the mid-plane, there is an identical ply (material and thickness) of ***-θ*** orientation below the mid-plane as shown in Fig. 2; the shear–normal coupling effect is eliminated. However, if the shaft is made from laminates to provide a single winding angle, then shear–normal coupling (due to the terms $\bar{Q}_{16} \neq 0$ and $\bar{Q}_{26} \neq 0$) will be present. Generally, coupling exists between normal stress (***σ**xx*) with shear strain (***ε**xθ*) and shear stress (***τ**xθ*) with normal strain (***ε**xx*). From the classical laminate theory, the forces on the laminate are related with strain as follows

$$\{N\} = \left[A_{ij}\right]\{\varepsilon\} \tag{17}$$

or

$$\{\varepsilon\} = \left[A_{ij}\right]^{-1}\{N\} \tag{18}$$

For a uniaxial load in longitudinal direction and laminate of total thickness ***t***, ***N**xx* = ***tσ**xx*; ***N**θθ* = ***0***; and ***N**xθ* = ***0***: Then

$$\varepsilon_{xx} = \frac{a\sigma_{xx}^{t}}{\Delta} \text{ or } \frac{\sigma_{xx}}{\varepsilon_{xx}} = E_{xx} = \frac{\Delta}{at}$$

where ***Δ** = **A**11**a** - **A**12**b** + **A**16**c*** and ***a, b*** and ***c*** are the cofactors of ***A**11, **A**12*** and ***A**16*, respectively given by

$$a = A_{22}A_{66} - A_{26}^2 \text{ for single ply k, } a^k = \bar{Q}_{22}^k\bar{Q}_{66}^k - \left(\bar{Q}_{26}^k\right)^2$$

$$b = A_{12}A_{66} - A_{16}A_{26} \text{ for single ply k, } b^k = \bar{Q}_{12}^k\bar{Q}_{66}^k - \bar{Q}_{16}^k\bar{Q}_{26}^k$$

$$c = A_{12}A_{26} - A_{16}A_{22} \text{ for single ply k, } c^k = \bar{Q}_{12}^k\bar{Q}_{26}^k - \bar{Q}_{16}^k\bar{Q}_{22}^k$$

The longitudinal and shear moduli can be given by

$$E_{xx} = \frac{\sigma_{xx}}{\varepsilon_{xx}} = \left(\frac{A_{11}a - A_{12}b + A_{16}c}{at}\right) \tag{19}$$

Similarly, applying $N_{x\theta}$ and keeping ***N**xx* = ***N**θθ* = ***0***; one obtains

$$G_{x\theta} = \frac{\tau_{xy}}{\varepsilon_{xy}} = \left(\frac{A_{11}a - A_{12}b + A_{16}c}{ft}\right) \tag{20}$$

where $\boldsymbol{f = A_{11}A_{22} - A_{12}^2}$, for single ply k, $\boldsymbol{f^k = \bar{Q}_{11}^k \bar{Q}_{22}^k - \left(\bar{Q}_{12}^k\right)^2}$.

Taking a configuration of single ply, then Eqs. (19) and (20) become

$$E_{xx} = \frac{\sigma_{xx}}{\varepsilon_{xx}} = \left(\frac{\bar{Q}_{11}a^k - \bar{Q}_{12}b^k + \bar{Q}_{16}c^k}{a^k}\right) \tag{21}$$

and

$$G_{x\theta} = \frac{\tau_{xy}}{\varepsilon_{xy}} = \left(\frac{\bar{Q}_{11}a^k - \bar{Q}_{12}b^k + \bar{Q}_{16}c^k}{f^k}\right) \tag{22}$$

To account for shear–normal coupling effect, the value of $\boldsymbol{\bar{Q}_{11}^k}$ in Eq. (14) and the value of $\boldsymbol{G_{x\theta}}$ in calculating $\boldsymbol{ks}$ are replaced by $\boldsymbol{E_{xx}}$ and $\boldsymbol{G_{x\theta}}$ obtained in Eqs. (19) and (20), respectively. For symmetric balanced laminate or orthotropic plies, the terms $\boldsymbol{\bar{Q}_{16}}$ and $\boldsymbol{\bar{Q}_{26}}$ vanish and Eqs. (19) and (20) can be re-written as

$$E_{xx} = \frac{\left(A_{11} - \frac{A_{12}^2}{A_{22}}\right)}{t} \tag{23}$$

Similarly $G_{x\theta}$ reduces to

$$G_{x\theta} = \frac{A_{66}}{t} \tag{24}$$

For single ply, Eqs. (22) and (24) become

$$E_{xx} = \left(\bar{Q}_{11} - \frac{\left(\bar{Q}_{12}^k\right)^2}{\bar{Q}_{22}}\right) \tag{25}$$

And

$$G_{x\theta} = \bar{Q}_{66}^k \tag{26}$$

Eqs. (22) and (24) are similar to that of Singh and Gupta [28], used to evaluate equivalent modulus in EMBT. However, Eq. (25) is similar to Eq. (16) for updating the value of $\bar{Q}_{11}$ to account for Poisson's effect. It is to be noted that, in the present formulation, Poisson's effect is inherently included in the formulation of shear–normal coupling. This is clear by substituting ($\bar{Q}_{16} = \bar{Q}_{26} = 0$) for 0^o and 90^o ply angles in Eqs. (19) and (20) which reduce to Eqs. (16) and (23) and (26).

3.3.3. Improvement to Include Bending–Twisting Coupling Effect

In configurations at which $\boldsymbol{+\theta}$ orientations are above the mid-plane there is an identical lamina (in the thickness and material) of -θ orientation at the same distance below the mid-plane (as shown in Fig. 2), the bending–twisting coupling represented by the terms $\boldsymbol{D_{16}}$ and $\boldsymbol{D_{26}}$ (in the bending stiffness matrix [D]) for the laminate is zero. For symmetric laminate the terms $\boldsymbol{D_{16}}$ and $\boldsymbol{D_{26}}$ cannot be zero unless $\boldsymbol{\theta = 0^o}$ or $\boldsymbol{90^o}$. The bending–twisting stiffness coefficient [27] is given by

$$k_{BT} = \sum_{k=1}^{n} \bar{Q}_{16}^{(k)} \left[R_{(k)}^4\right] \tag{27}$$

The expression for strain energy is modified as

$$U = \frac{1}{2}\int_0^l \left\{ k_B \left[\left(\frac{\partial \alpha}{\partial x}\right)^2 + \left(\frac{\partial \beta}{\partial x}\right)^2 \right] + k_S \left[\left(\frac{\partial w}{\partial x} - \alpha\right)^2 + \left(\frac{\partial v}{\partial x} - \beta\right)^2 \right] + \frac{k_{BT}}{2} \left[\left(\frac{\partial \phi}{\partial x}\right)\left(\frac{\partial \alpha}{\partial x}\right) + \left(\frac{\partial \phi}{\partial x}\right)\left(\frac{\partial \beta}{\partial x}\right) \right] + k_T \left(\frac{\partial \phi}{\partial x}\right)^2 \right\} dx \quad (28)$$

4. Experimental Investigation

In the present experimental part the measurements of laminated composite shaft for various five lamina orientations, three different fiber volume fraction ratio, various (L/D) ratios and four boundary fixations are constructed and manufactured using winding layup method. The boundary conditions of a rotating composite shaft were achieved using a combination of various bush width and a rate level of bearing clearance to obtain a proper boundary fixation state.

The dynamic analysis in the experimental results in qualitative and quantitative manner is presented to investigate their dynamic eigen-parameters including natural frequencies and damping factors.

4.1. Composite Shaft Specimen Preparations

Figure 4 shows the rotating composite shaft manufacture at various types of lamina orientations angles. The preparation and manufacturing of specimens are achieved by following the standard procedures [29]. Five layers of ***(1mm)*** thickness were wind by the required angle and spread on a wood Die at various orientation fibers. A layer of resin is spread on a wood Die treated by release agent (Wax or medical Vaseline). The wood Die (***1000 long × 20 mm diameters***) is then placed on the glass fiber and assembly together by copper wire and to close gab by cement. The press die was removed after ***24 hours*** and the laminate has been completely cured at room temperature. The laminate composite shafts are cut to the required length (***800mm long***) using mechanical fine sawing machines.

Fig. 4 Composite shafts manufacture.

4.2. Experimental Modal of Vibration Damping of Composite Shaft FRP

The frequency response tests were performed on composite shaft made from fiber reinforced plastic (FRP) by utilizing fast Fourier transform dual channel analyzer in conjunction with the computer as shown in Fig.5**.**The corresponding fundamental frequency and damping factor for various lamina orientation and different boundary conditions are measured and recorded using (FFT) analyzer in the range of (***800:1600 Hz***).The comparison between theoretical analysis using (EMBT) and Experimental measurements were performed and listed of Tables 4.

Table 4 Comparison of natural frequencies (Hz) including different coupling effects at (L/D) ratio 40 with fiber volume fraction 65%

Play angle	Bending–twisting (only)	Poisson's effect (only)	Poisson's effect and bending–twisting	Shear–normal (only)	Including all coupling
	(1)	(2)	(3)	(4)	(5)
[0°]	119.47	119.47	119.47	119.47	119.47
[15°]	108.97	108.97	100.38	95.58	78.85
[30°]	73.14	73.14	72.66	53.54	51.915
[45°]	44.91	44.91	58.78	45.12	47.76
[60°]	34.41	34.41	41.09	32.64	36.96
[75°]	33.12	33.12	32.91	30.96	31.66
[90°]	31.54	31.54	31.54	31.54	31.54

The peak response frequencies were identified from the peaks in the frequency spectra FRS.

In addition, the system damping ratio $\boldsymbol{\xi}$ was evaluated from the quality factor $\boldsymbol{Q}$ from $\boldsymbol{\omega_1}$ and $\boldsymbol{\omega_2}$corresponding to half-power bandwidth method (29) as: [30]

$$Q \approx \frac{1}{2\xi} \approx \frac{\omega_n}{\omega_2 - \omega_1} \tag{29}$$

4.3. Eigen Parameter Measurements

The equation of motion of a damped multi degree of freedom system in matrix form:

$$[M]_e\{\ddot{X}\} + [C]_e\{\dot{X}\} + [K]_e\{X\} = \{F\} \tag{30}$$

By expressing the solution of {X} as a linear combination of the natural modes of the system as:

$$X = x\cos(\omega t) \tag{31}$$

For the applied harmonic force of $F = F_0\cos(\omega t)$ at the rotating composite shaft.

By substituting Eqn. (31) into Eqn. (30), we obtain

$$\{x\} = [-\omega^2[M]_e + j\omega[C]_e + [K]_e]^{-1}\{F_0\} \tag{32}$$

$$[C]_d = \gamma[M]_e + \lambda[K]_e \tag{33}$$

$$[C]_d[K]_e{}^{-1}[M]_e = [M]_e[K]_e{}^{-1}[C]_d \tag{34}$$

$$\xi_i = \frac{\gamma}{2\omega_i} + \frac{\lambda\omega_i}{2} \tag{35}$$

The eigen value problem of proportional damped system can be resolved to two stander eigen value problem [31] and the form.

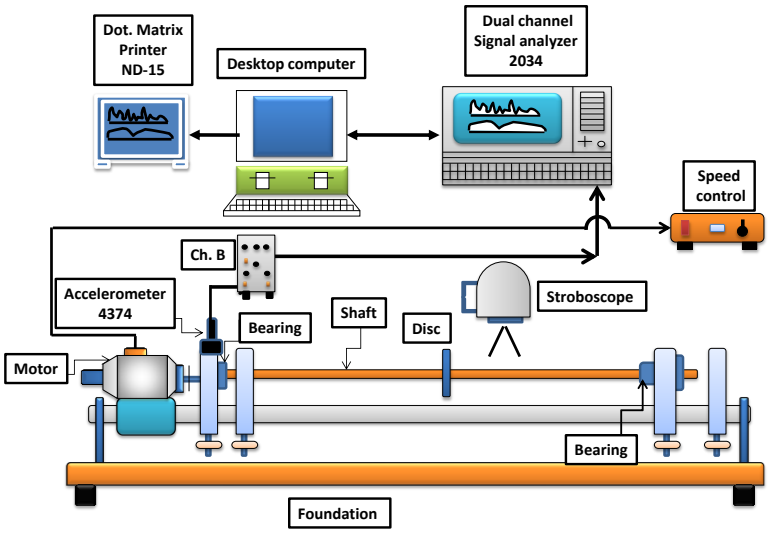

(a) Schematic diagram

(b) Photograph

Fig. 5 The TM1 MKII Whirling of shafts apparatus connected with dual channel analyzer test

$$\left[[M]_e^{-1}[K]_e - \omega^2[I]\right] = 0 \tag{36}$$

$$\left[[M]_e^{-1}[C]_e - u[I]\right] = 0 \tag{37}$$

The equivalent damping matrix $[C]_e$ can be calculated as a proportional damping (Rayleigh damping) as shown in Eqn. (33), where γ and λ are coefficients determined by experimental investigation. The necessary and sufficient conditions of proportional damping system are given by Eqn. (34). In this case, the response of the rotating composite shaft was separated into the responses at each mode by spectral analysis and the damping ratio ξ_i and coefficients γ and λ are identified by Eqn. (35). The results of the coefficients γ and λ are listed in Table 4 where:

ξ_i and ω_i are the damping ratio and natural frequency of i^{th} mode respectively and u is the eigen values of inertia damping matrix, $u = 2\xi\omega$.

To study the effect of fiber orientation on the dynamic behavior of laminate composite shaft. The specimen location in the ***TM1*** whirling of shafts apparatus and the boundary conditions can be achieved using suitable bearing then the ratio of clearance and bush bearing width adjustable.

5. Results and Discussion

5.1 Effect of Stacking Sequences, *(L/D)* Ratios, Boundary Conditions and Fiber Volume Fraction on Eigen Frequency.

Figure 6 shows the effect of stacking sequences, ***(L/D)*** ratios, different types of boundary conditions on frequency value based on mathematical modeling under fiber volume fraction V_f **= *65%.*** From Fig. 6 it can be notes that the frequency values significantly varied with the state of stacking sequences. This is due to the outer staking layer is more effect on the stiffness compared with the inner layer. The change of lamina orientations from ***[0/0/0/0/0]*** to ***[90/90/0/90/90]*** decreases the eigen frequency by ***54.42%***.

From Table 3 the effect of fiber volume fraction is slightly effect on the eigen parameters this indicate in the specimen ***[0/0/0/0/0]*** and volume fraction ***65%***, frequency values slightly increase. The low value of frequency at ***[90/90/0/90/90]*** and volume fraction 25% may be attributed to the low level of potential energy at this condition.

In view of lamina orientations, the rate of change of the frequency via fiber volume fraction are relatively high compared with the rate of change due lamina orientations as shown in Table 3. From Fig.6 it can be observed that specimen ***[90/90/0/90/90]*** has the lowest frequency compared with the other specimen while the specimen [0]5 has the highest values this is due to the minimum and maximum values of flexural elastic modules and stiffness at this orientation respectively. The change of lamina orientations from ***[0/0/0/0/0]*** to ***[0/90/0/90/0]*** decreases by ***54.4%***.

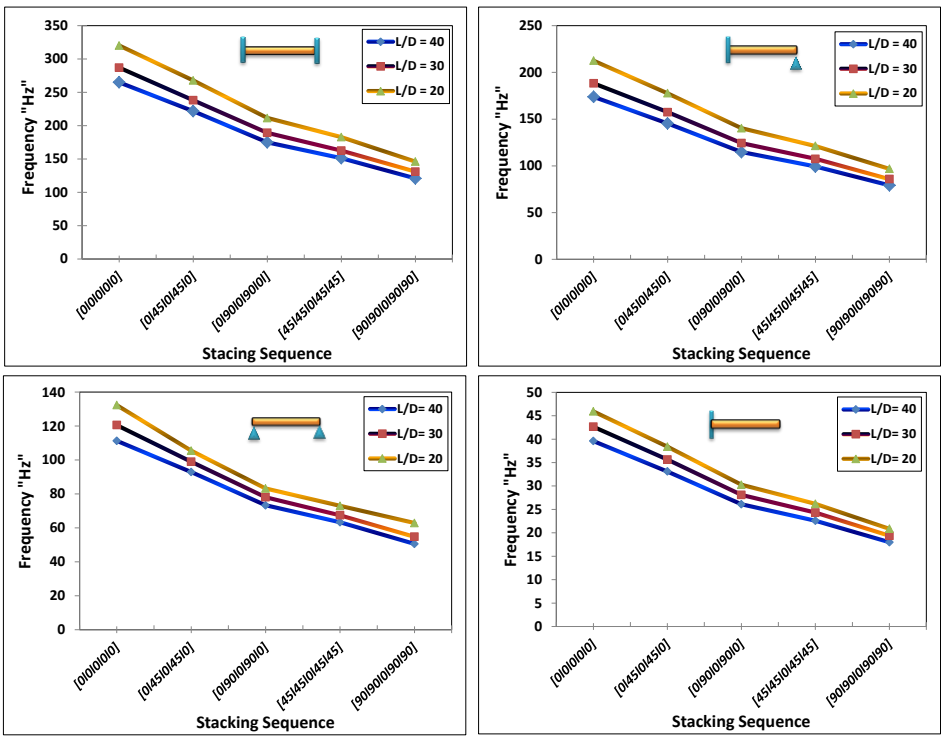

Fig. 6 Effect of stacking sequence on frequency at different (*L/D*) ratios and various boundary fixations with fiber volume fraction *Vf = 65%*.

From Table 3 (a), (b) and (c) it can be noted that, the fiber volume fraction has a limited effect on frequency and damping factor value because the effect of lamina orientations has a dominant influence.

Table 3 Values of fundamental frequency in Hz and damping factor "ξ" for various laminated orientations, fiber volume fraction and different boundary fixation*

a. (L/D = 40)

Lamina orientation and boundary fixations		C-C				C-S				S-S				C-F			
		Ξ	f, [Hz]			ξ	f, [Hz]			ξ	f, [Hz]			ξ	f, [Hz]		
			EMBT	FE	Ex		EMBT	FE	Ex		EMBT	FE	Ex		EMBT	FE	Ex
[0/0/0/0/0]	V_f = 25%	0.11	264.8	261	260	0.13	173.7	172	167	0.14	111.3	111	109	0.17	39.6	38	37
[0/45/0/45/0]		0.14	221.5	220	219	0.15	145.2	144	141	0.16	92.9	90	87	0.19	33.1	33	29
[0/90/0/90/0]		0.19	174.8	172	170	0.22	114.6	113	111	0.24	73.3	73	70	0.34	26.1	25	22
[45/45/0/45/45]		0.22	151.1	149	148	0.29	99.1	99	87	0.32	63.3	62	59	0.40	22.6	22	18
[90/90/0/90/90]		0.28	120.7	119	117	0.33	79.1	78	75	0.36	50.6	50	46	0.47	18.0	17	14
[0/0/0/0/0]	V_f = 45%	0.09	320.4	320	318	0.11	210.1	209	208	0.14	131.3	131	129	0.17	47. 1	46	44
[0/45/0/45/0]		0.12	268. 1	266	263	0.14	173.6	172	169	0.15	114.4	114	113	0.19	40. 1	39	38
[0/90/0/90/0]		0.15	211.5	211	207	0.18	136.4	135	134	0.21	87. 3	87	85	0.29	31.5	30	29
[45/45/0/45/45]		0.19	182. 3	180	177	0.23	116.2	116	115	0.27	76. 3	75	74	0.36	27.3	27	26
[90/90/0/90/90]		0.24	145. 4	143	140	0.29	93. 1	92	90	0.31	62.2	61	60	0.42	21.3	21	20
[0/0/0/0/0]	V_f = 65%	0.06	396.2	395	392	0.09	258.4	257	255	0.13	164.3	163	161	0.16	58.4	56	56
[0/45/0/45/0]		0.10	328.1	328	326	0.11	216.3	216	214	0.15	137.1	137	135	0.18	48. 2	45	43
[0/90/0/90/0]		0.13	257.3	254	253	0.16	167.1	166	163	0.18	108.2	108	105	0.23	38.1	37	35
[45/45/0/45/45]		0.16	226.2	224	224	0.19	144.2	144	141	0.23	93.4	92	89	0.29	33.3	33	30
[90/90/0/90/90]		0.19	175.4	174	172	0.23	113.7	112	109	0.29	74. 2	73	71	0.34	26.5	26	24

b. (L/D = 30)

Lamina orientation and boundary fixations		C-C				C-S				S-S				C-F			
		ξ	f, [Hz]			ξ	f, [Hz]			ξ	f, [Hz]			ξ	f, [Hz]		
			EMBT	FE	Ex		EMBT	FE	Ex		EMBT	FE	Ex		EMBT	FE	Ex
[0/0/0/0/0]	V_f = 25%	0.09	286.8	286	283	0.12	188.2	187	186	0.13	120.5	120	117	0.15	46.2	45	44
[0/45/0/45/0]		0.13	237.9	235	234	0.14	157.3	156	154	0.15	109.7	107	106	0.17	38.6	37	35
[0/90/0/90/0]		0.17	186.3	185	182	0.20	124.3	124	121	0.21	76.2	75	73	0.31	30.4	30	27
[45/45/0/45/45]		0.20	162.3	160	158	0.26	107.3	107	104	0.28	65.9	65	62	0.36	26.3	25	23
[90/90/0/90/90]		0.26	130.7	130	127	0.29	85. 7	85	83	0.32	54.8	53	51	0.42	21.0	20	17
[0/0/0/0/0]	V_f = 45%	0.08	344.0	343	341	0.10	227.6	227	225	0.12	142.2	140	138	0.15	67.1	66	64
[0/45/0/45/0]		0.11	281.6	280	277	0.12	188.1	117	184	0.14	123. 3	122	120	0.17	45.5	45	43
[0/90/0/90/0]		0.14	220.3	220	218	0.16	147.7	146	144	0.19	99.3	98	96	0.26	36.7	35	33
[45/45/0/45/45]		0.18	199.1	199	196	0.20	125.8	124	122	0.24	72.4	70	70	0.32	31.8	30	28
[90/90/0/90/90]		0.22	171.4	171	168	0.25	100.3	100	198	0.27	67.4	66	64	0.38	24.8	23	21
[0/0/0/0/0]	V_f = 65%	0.05	418.7	417	415	0.08	279.9	279	277	0.12	177.9	175	173	0.14	68.1	67	66
[0/45/0/45/0]		0.09	358.2	357	356	0.10	234.3	233	231	0.14	148.5	146	145	0.16	53.2	52	51
[0/90/0/90/0]		0.12	274.3	274	270	0.14	181.0	180	179	0.16	117.1	116	114	0.20	44.4	44	40
[45/45/0/45/45]		0.15	242.8	242	239	0.17	156.2	155	153	0.21	101.1	100	97	0.26	38.8	38	36
[90/90/0/90/90]		0.17	188.4	187	185	0.20	123.2	123	120	0.25	84.3	83	81	0.31	30.9	30	27

Table 3 (*Continued)*
c. (L/D = 20)

Lamina orientation and boundary fixations		C-C				C-S				S-S				C-F			
		ξ	f, [Hz]			ξ	f, [Hz]			ξ	f, [Hz]			ξ	f, [Hz]		
			EMBT	FE	Ex		EMBT	FE	Ex		EMBT	FE	Ex		EMBT	FE	Ex
[0/0/0/0/0]	V_f = 25%	0.08	308. 3	307	305	0.11	219.5	218	216	0.12	140.6	139	137	0.14	53.9	52	50
[0/45/0/45/0]		0.11	260.2	259	257	0.13	183.5	182	180	0.14	128.1	126	125	0.15	45.2	44	43
[0/90/0/90/0]		0.15	202.2	201	200	0.17	144.8	144	142	0.19	88.2	87	86	0.27	35.5	33	32
[45/45/0/45/45]		0.17	176.1	175	174	0.23	125.2	124	123	0.25	76. 3	76	75	0.32	30.7	30	28
[90/90/0/90/90]		0.22	141.6	141	140	0.26	99.9	99	97	0.28	63. 78	62	60	0.38	24.5	23	22
[0/0/0/0/0]	V_f = 45%	0.07	373.8	373	370	0.09	265.5	265	263	0.11	165. 1	163	162	0.13	73.2	72	70
[0/45/0/45/0]		0.10	313.2	312	311	0.11	219.4	218	216	0.13	144.5	143	141	0.15	61.1	60	60
[0/90/0/90/0]		0.12	246.7	245	244	0.14	172.3	172	170	0.17	121.3	119	118	0.23	42. 5	41	40
[45/45/0/45/45]		0.16	202.2	201	199	0.18	146.3	144	142	0.21	99.8	98	95	0.29	37.1	35	34
[90/90/0/90/90]		0.20	179.4	178	177	0.23	119.2	118	116	0.24	78.6	76	75	0.33	28.9	27	26
[0/0/0/0/0]	V_f = 65%	0.05	458.4	457	455	0.07	326.5	326	324	0.10	207.6	206	205	0.13	79.4	79	76
[0/45/0/45/0]		0.08	378.1	377	374	0.09	273.3	272	271	0.13	173.2	172	170	0.14	63.1	62	60
[0/90/0/90/0]		0.11	301.3	300	299	0.12	211.1	209	208	0.15	136.7	135	133	0.18	51. 3	50	48
[45/45/0/45/45]		0.13	257.4	256	255	0.15	182.2	180	178	0.18	118. 2	117	116	0.23	45.3	44	43
[90/90/0/90/90]		0.16	201.2	201	198	0.18	143.7	142	140	0.22	89.4	88	87	0.27	36. 4	34	33

* (C-C) = clamped-clamped, (C-S) = clamped-simply supported,
(S-S) = simply supported-simply supported, (C-F) = clamped-free

From Fig. 7 it can be observed that specimen ***[0/0/0/0/0]*** has the lowest damping factor compared with the other specimen while the specimen ***[90/90/0/90/90]*** has the highest values this is due to the minimum and maximum values of flexural elastic modules. In view of different fixation, the rate of change of the critical speed via different fixations are relatively high compared with the rate of change due to the use of the various code numbers of fiber orientations as shown in Fig. 6 (c) and Table 3.

Figure 7 declares the effect of stacking sequences and fiber volume fraction on damping factor under one case of clamped-clamped boundary fixation. It is clear that the damping factor values significantly varied with the state of lamina orientations and fiber volume fraction in a reverse trend as compared with frequency Fig. 6 (a). The high value of damping factor occurs under [0/90/0/90/0] and ***25%*** volume fraction.

5.2. Effect of Including Different Coupling Mechanism on Natural Frequency

Figure 8 shows the validation of formulation and programming, the results obtained from modified EMBT. In order to have a basis for comparison between different coupling mechanism effects. Results presented in Table 4, clearly show excellent agreement of the natural frequencies obtained from EMBT for shafts with single ply of fiber angle varying from 0^o to 90^o, fiber volume fraction is ***65%*** and ***(L/D)*** ratio ***40***. As expected, natural frequencies in the first modes are found to decrease with the value of fiber angle increasing from 0^o to 90^o**.** For excluding Poisson's and other coupling effects with changing the fiber angle ply from 0^o to 90^o the natural frequencies decreases by 69.6%. For including Poisson's and other coupling effects with changing the fiber angle ply from 0^o to 90^o the natural frequencies decreases by ***69.6%***.

5.3. Dynamic Response of Rotating Composite Shaft

Programming codes based Matlab program, version (7.1) are implemented to analyze the dynamic response of the rotating composite shaft under a harmonic load on the bases on the proposed theoretical investigations. The analysis are performed for composite shaft of three types of ***(L/D)*** ratio ***(20, 30 and 40)***, fiber volume fraction ***(65%)***, ***(S-S)*** boundary fixation and various types of lamina fiber orientations.

Figures 9 represent the frequency response of the composite shaft at the clamped-clamped boundary fixation of the specimen with various types of fiber volume fraction and various lamina fiber orientation angles. The results indicate that there is apparently a correlation between the theoretical and experimental results, Table 5, shows the damping factors, natural frequency for the first and second mode for three types of fiber volume fraction and various lamina orientations and the coefficients γ and λ.

The composite shaft is discretized into three interconnected elements using FEM. From Fig. 9 it can be seen that the amplitude of specimens [***90/90/0/90/90***] are higher than those of the other specimen and [***0/0/0/0/0***] has lower ones. And the maximum amplitude at ***(L/D = 40)*** compared with the ***(L/D = 20)*** by almost ***0.9%***. From the previous result it can be shown that the maximum amplitude at ***(L/D)*** ratio ***40*** and [***90/90/0/90/90***] specimens and minimum amplitude at ***(L/D) ratio 20*** and [***0/0/0/0/0***] specimens.

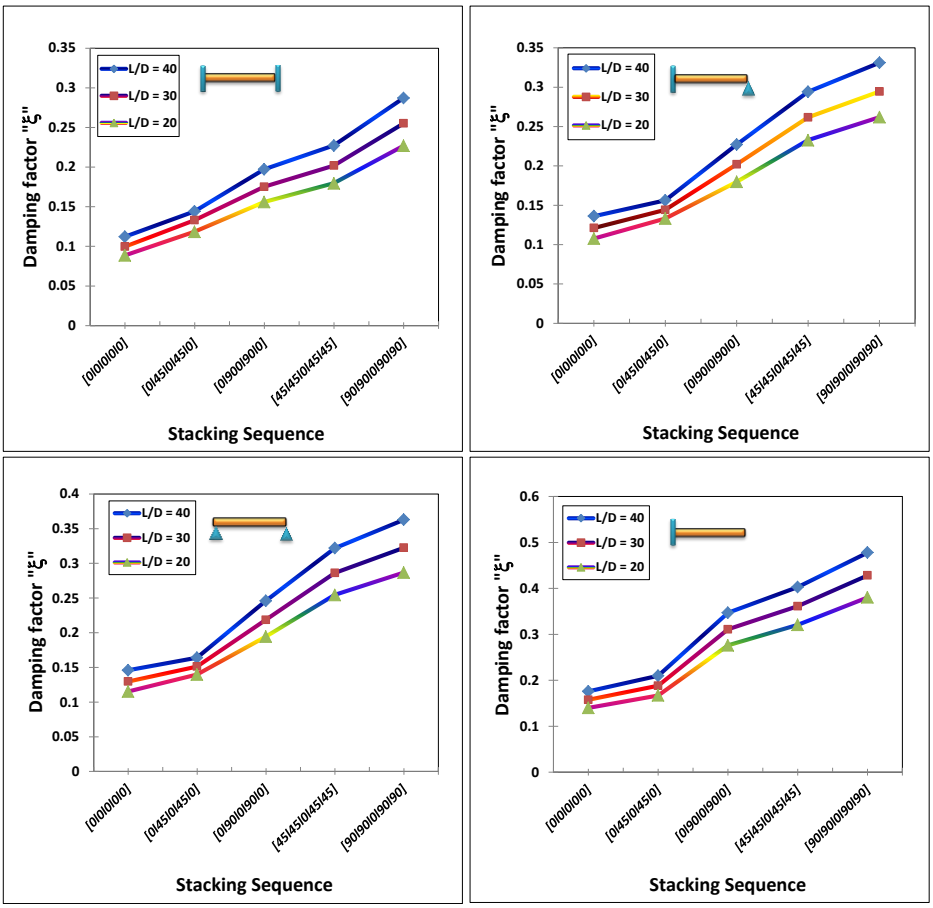

Fig. 7 Effect of stacking sequence on damping factor at different (*L/D*) ratios and various boundary fixations with fiber volume fraction *Vf = 65%*.

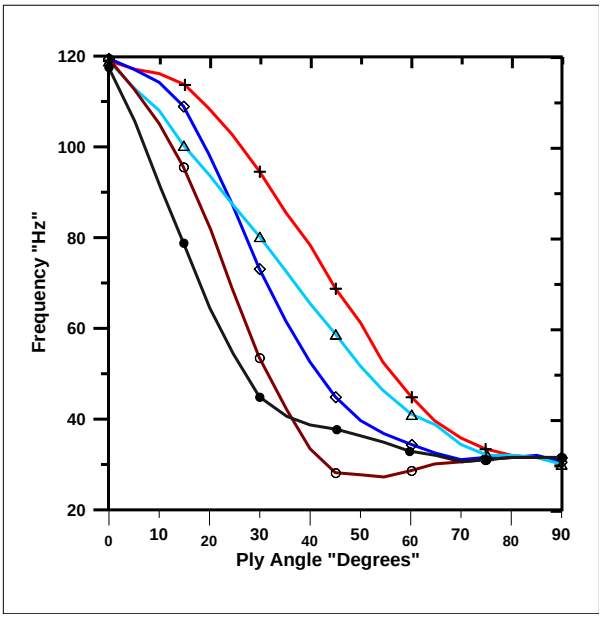

+ Bending–twisting (only); Δ Poisson's effect (only);
◊ Poisson's effect and bending–twisting; ○ Shear–normal (only);
● Including all coupling.

Fig. 8 Variation of natural frequency with different ply angles due to different coupling mechanisms.

Table 5 The damping factors, natural frequency and coefficients γ and λ for *(S-S)* boundary fixation with $V_f = 65\%$.

Lamina orientation		$_1\xi$	$_2\xi$	$_1\omega$	$_2\omega$	γ	λ
[0/0/0/0/0]	L/D = 40	0.13	0.107	164.3	398.2	39.38	$2.84*10^{-4}$
[0/45/0/45/0]		0.15	0.136	137.1	352.5	43.03	$4.23*10^{-4}$
[0/90/0/90/0]		0.18	0.191	108.2	285.3	44.76	$7.89*10^{-4}$
[45/45/0/45/45]		0.23	0.220	93.4	146.6	44.61	$1.1*10^{-3}$
[90/90/0/90/90]		0.29	0.281	74. 2	196.7	44.36	$1.7*10^{-3}$
[0/0/0/0/0]	L/D = 30	0.12	0.087	177.9	522.8	42.8	$1.76*10^{-4}$
[0/45/0/45/0]		0.14	0.122	148.5	437.5	44.85	$3.23*10^{-4}$
[0/90/0/90/0]		0.16	0.150	117.1	345.2	43.41	$5.05*10^{-4}$
[45/45/0/45/45]		0.21	0.177	101.1	297.5	42.93	$7.04*10^{-4}$
[90/90/0/90/90]		0.25	0.236	84.3	237.3	85.81	$1.2*10^{-3}$
[0/0/0/0/0]	L/D = 20	0.10	0.053	207.6	672.9	5.59	$2.72*10^{-4}$
[0/45/0/45/0]		0.13	0.101	173.2	540.9	45.41	$2.18*10^{-4}$
[0/90/0/90/0]		0.15	0.128	136.7	431.2	46.04	$3.46*10^{-4}$
[45/45/0/45/45]		0.18	0.162	118. 2	385.3	51.01	$4.97*10^{-4}$
[90/90/0/90/90]		0.22	0.190	89.4	323.8	46.21	$7.33*10^{-4}$

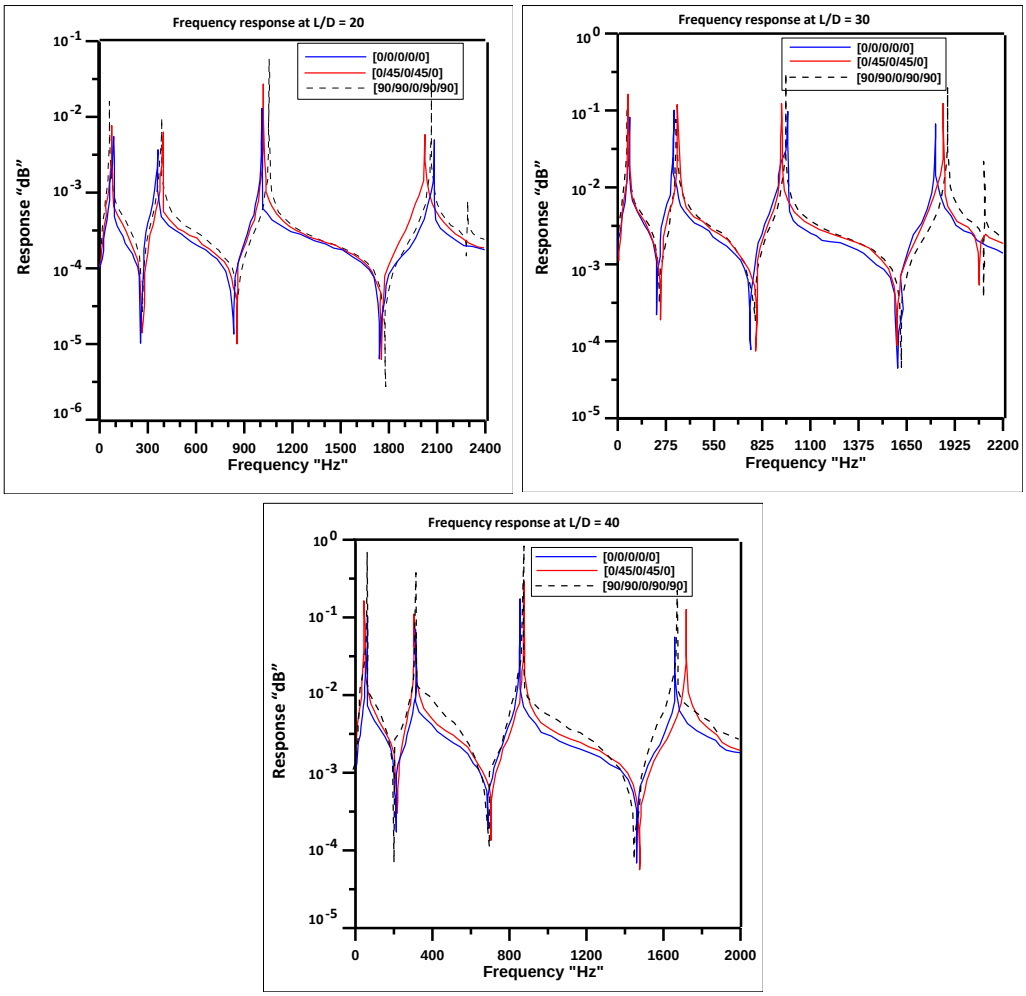

Fig. 9 Results of the theoretical model for the frequency response of the rotating composite shaft at (S-S) boundary fixation and fiber volume fraction 65%.

6. Conclusions

From the numerical and experimental results one can conclude:

The dynamic analysis of laminated composite shaft with different stacking sequences, five cases will be studied using composite shafts wounded by different layers of composite materials namely; different stacking sequence, fiber orientation angles, (***L/D***) ratio, boundary condition and finally various types of fiber volume fraction.

i. The present comparison between the numerical and experimental results proves that the suggested finite element models of the composite structural shaft, bearing and disc with current fixations state provide an efficient tool for compute the dynamic analysis with proper accuracy.

ii. Dynamic response gives proper information about resonance avoidance for certain operation conditions particularly composite shaft. In the other hand frequency response of composite shaft provides proper indication about vibration state and the location of nodes and modes at each position. These important parameters from designers point of view.

iii. It can be concluded that inclusion of layer along the transverse direction into fiber/polyester material is a good option for manufacturing stiffer shafts.

iv. Different coupling mechanisms, as obtained from (EMBT) theory, were found to reduce shaft natural frequencies. The percentage reduction depends on coupling mechanisms available in different ply angles. For Poisson's effect the maximum reduction in the shaft natural frequency is found to be at about 45^o ply angle, however for shear–normal and bending–twisting coupling, the maximum reduction is found to be at about 30^o ply angle.

References

[1] Tan C. A. and Kuang, W., "Vibration of a Rotating Discontinuous Shaft by the Distributed Transfer Function Method", Journal of Sound and Vibration, Vol. 183(3),1995, pp. 451-474.

[2] Bolotin V. V., "Nonconservative Problems of the Theory of Elastic Stability", [New York] Macmillan, 1963.

[3] Grybos R., "Effect of shear and rotary inertia of a rotor at its critical speeds", Archive of Applied Mechanics, Vol. 61 (2), 1991, pp. 104–109.

[4] Choi S.H., Pierre C .and Ulsoy A.G., "Consistent modeling of rotating Timoshenko shafts subject to axial loads", Journal of Vibration, Acoustics, Stress, and Reliability in Design, Vol. 114 (2), 1992, pp. 249–259.

[5] Jei Y.G. and Leh C.W., "Modal analysis of continuous asymmetrical rotor-bearing systems", Journal of Sound and Vibration, Vol. 152 (2), 1992, pp. 245–262.

[6] Singh S.P. and Gupta K., "Free damped flexural vibration analysis of composite cylindrical tubes using beam and shell theories", Journal of Sound and Vibration, Vol. 172 (2), 1998, pp. 171–190.

[7] Sturla F.A. and Argento A., "Free and forced vibrations of a spinning viscoelastic beam", Journal of Vibration and Acoustics, Vol. 118 (3), 1996, pp. 463–468.

[8] Melanson J. and Zu J.W., "Free vibration and stability analysis of internally damped rotating shafts with general boundary conditions", Journal of Vibration and Acoustics, Vol. 120 (3), 1998, pp. 776–783.

[9] Kim W., Argento A. and Scott R.A., "Free vibration of a rotating tapered composite Timoshenko shaft", Journal of Sound and Vibration, Vol. 226 (1), 1999, pp. 125–147.

[10] Hosseini S.A. and Khadem S.E., "Free vibrations analysis of a rotating shaft with nonlinearities in curvature and inertia", Mechanism and Machine Theory, Vol. 44, 2009 pp. 272–288.

[11] Newkirk, "Shaft whipping". Gen Electric Rev, Vol. 27(3), 1924, pp. 169–178.

[12] AL. Kimball, "Internal friction as a cause of shaft whirling". Philos Mag, Vol. 49(1), 1925 pp. 724.

[13] Bucciarelli LL., "On the instability of rotating shafts due to internal damping". J Appl Mech, Vol. 49, 1982, pp. 425.

[14] Tsaı SW., "Composites design". 4th ed. Ohio, USA: Dayton; 1988.

[15] Rastogi N. "Design of composite driveshafts for automotive applications", SAE, technical paper series, 2004.

[16] Shokrieh Mahmood M, Hasani Akbar, Lessard Larry B., "Shear buckling of a composite drive shaft under torsion", Compos Struct., 2004, pp. 64:63.

[17] Topal Umat. "Multi objective optimization of laminated composite cylindrical shells for maximum frequency and buckling load", Mater Des., Vol. 30(7), 2009, pp. 2584–2594.

[18] Silvestre N., "Generalized beam theory to analyze the buckling behavior of circular cylindrical shells and tubes", Thin-Walled Struct. Vol. 45(2), 2007, pp. 185–198.

[19] Bert CW. and Kim CD., "Analysis of buckling hollow laminated composite drive shafts", Compos Sci. Technol. 1995;53:343–51.

[20] Chen LW, Kung Peng W., "The stability behavior of rotating composite shafts under axial compressive loads", Compos Struct., Vol. 41, 1998, pp. 253–263.
[21] Badie M.A., Mahdi E. and Hamouda A.M.S., "An investigation into hybrid carbon/glass fiber reinforced epoxy composite automotive drive shaft", Materials and Design, Vol. 32, 2011, pp. 1485–1500.
[22] Tita V., Carvalho J. and Lirani J., "Theoretical and experimental dynamic analysis of fiber reinforced composite beams", J. of the Braz. Soc. Mech. Sci. 7 Eng. XXV, Vol. 3.2003, p. 306.
[23] Ghoneam S. M., Hamada A. A. and EL-Elamy M. I., "Experimental and Analytical Investigations of the Dynamic Analysis of Adhesively Bonded Joints for Composite Structures", Solid State Phenomena Vols. 147-149, 2009, pp. 663-675.
[24] Richardet J., Chatelet E. and Lornage D., "A three dimensional modeling of the dynamic behavior of composite rotors", Proceedings of ISROMAC-8 (The 8th International Symposium on Transport Phenomena and Dynamics of Rotating Machinery), March 2000, Honolulu, Hawaii, USA,2000, pp. 988–994.
[25] Gubran H.B.H., "Dynamics of hybrid shafts, Mechanics Research Communications", Vol. 32, 2005, pp. 368–374.
[26] Lalanne M. and Ferraris G., "Rotordynamics Prediction in Engineering", (1990).
[27] Gubran H.B.H .and Gupta K., " The effect of stacking sequence and coupling mechanisms on the natural frequencies of composite shafts", Journal of Sound and Vibration, Vol. 282, 2005, pp. 231–248.
[28] Singh S.P. and Gupta K., "Composite shaft rotordynamic analysis using a layerwise theory", Journal of Sound and Vibration, Vol. 191 (5), 1996, pp. 739 –756.
[29] Kristin Z. and Dahsin L., "Geometrical parameters in composite repair", Journal of Composite Materials, Vol. 29, (11),1995, p. 1473.
[30] Rao S., "Mechanical Vibrations", SI Edition, Prentice Hall, New York, 2004.
[31] A. Maher, "Notes on Dynamic of machine", Printed Lecture, 2000, p. 3-3 – 3-4.